Journal of Colloid and Interface Science 553 (2019) 390–401

Contents lists available at ScienceDirect

Journal of Colloid and Interface Science

journal homepage: www.elsevier.com/locate/jcis

Regular Article

Singlet oxygen photo-production by perylene bisimide derivative Langmuir-Schaefer films for photodynamic therapy applications

Paola Semeraro [a,1], Zois Syrgiannis [b,1], Simona Bettini [c,d,*], Gabriele Giancane [c,e], Flora Guerra [a], Aurore Fraix [f], Cecilia Bucci [a], Salvatore Sortino [f], Maurizio Prato [g,h,i,*], Ludovico Valli [a,c]

[a] Department of Biological and Environmental Sciences and Technology (DiSTeBA), Campus University Ecotekne, University of Salento, Via per Monteroni, I-73100 Lecce, Italy
[b] Simpson Querrey Institute for BioNanotechnology, Northwestern University
[c] Consorzio Interuniversitario Nazionale per la Scienza e Tecnologia dei Materiali, INSTM, Via G. Giusti, 9, I-50121 Firenze, Italy
[d] Department of Engineering for Innovation, Campus University Ecotekne, University of Salento, Via per Monteroni, I-73100 Lecce, Italy
[e] Department of Cultural Heritage, University of Salento, Via D. Birago 84, I-73100 Lecce, Italy
[f] Laboratory of Photochemistry, Department of Drug Sciences, University of Catania, Viale Andrea Doria 6, I-95125 Catania, Italy
[g] Center of Excellence for Nanostructured Material (CENMAT) and INSTM, Unit of Trieste, Department of Chemical and Pharmaceutical Science, University of Trieste, Via L. Giorgieri 1, 34127 Trieste, Italy
[h] Carbon Bionanotechnology Laboratory, CIC biomaGUNE, Paseo de Miramon 182, 20009 Donostia-San Sebastian, Spain
[i] Basque Fdn Sci, Ikerbasque, 48013 Bilbao, Spain

GRAPHICAL ABSTRACT

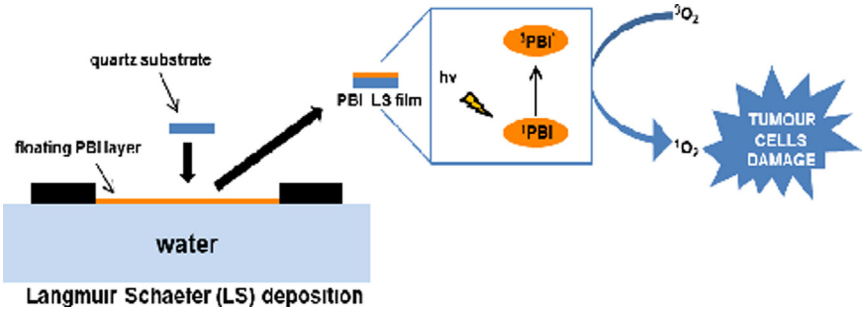

ARTICLE INFO

Article history:
Received 19 March 2019
Revised 6 June 2019
Accepted 11 June 2019
Available online 12 June 2019

Keywords:
Perylene bisimide derivative
Langmuir-Schaefer films
Singlet oxygen production
Photoactive device
Photodynamic therapy applications

ABSTRACT

A perylene bisimide (PBI) derivative was utilized as photosensitizer for photodynamic therapy (PDT) applications, due to its high efficiency in singlet oxygen generation upon photoexcitation. It was immobilized onto a hydrophobized solid support, by means of the Langmuir-Schaefer (LS) technique, to achieve a preliminary medical device able to induce death of cancer cells in vitro. First, PBI derivative solutions, at two different concentrations (4.2×10^{-5} and 1.5×10^{-4} M) were chosen, based on the different PBI aggregation state, to be spread onto a water subphase in a Langmuir trough. Physico-chemical and morphological characterizations of the floating films were performed. Then the floating layers were transferred onto quartz substrates. The resulting multilayer LS films were characterized by spectroscopic measurements showing that the photochemical properties of the PBI derivative were well preserved even when immobilized. The LS film that exhibited the highest efficiency in the singlet oxygen production under light excitation was assessed in *in vitro* tests on human cervical carcinoma C13 cell line and the

* Corresponding authors at: Consorzio Interuniversitario Nazionale per la Scienza e Tecnologia dei Materiali, INSTM, Via G. Giusti, 9, I-50121 Firenze, Italy; Department of Engineering for Innovation, Campus Universuty Ecotekne, University of Salento, Via Monteroni, I-73100, Lecce, Italy (S. Bettini) and Center of Excellence for Nanostructured Material (CENMAT) and INSTM, Unit of Trieste, Department of Chemical and Pharmaceutical Science, University of Trieste, Via L. Giorgieri 1, 34127 Trieste, Italy (M. Prato).
E-mail addresses: simona.bettini@unisalento.it (S. Bettini), prato@units.it (M. Prato).
[1] These authors equally contributed.

https://doi.org/10.1016/j.jcis.2019.06.037

photo-toxicity was measured. This study revealed absence of cytotoxicity in dark conditions and a high photo-cytotoxicity toward cancer cells, making it a promising photoactive device.

1. Introduction

Perylene bisimide (PBI) derivatives constitute a class of dyes with outstanding optoelectronic properties which have been examined in a very large scale last years [1]. These compounds are intensively used for different applications [1,2], due to their high chemical and thermal stability, high fluorescence quantum yield and large absorption coefficient [3,4]. They have been, indeed, already used for organic electronic employments [5–7], such as photovoltaic cells [8,9], as selective sensing devices for aromatic amines [10,11] or toxic gases [12,13] and as probes for biological macromolecules, such as proteins, DNA or RNA [1,14].

Due to triplet state formation of many PBI derivatives, upon photo-excitation process [15], these compounds are demonstrated to have high efficiency in the generation of singlet oxygen ($^1O_2$) [16,17]. In the presence of molecular oxygen, the energy stored in PBI excited states could be transferred to the ground state of molecular oxygen, leading to $^1O_2$, a highly reactive species [18–20].

These peculiarities of PBI derivatives make them interesting and promising candidates for the development of highly efficient and photo-stable photosensitizers (PSs) for Photodynamic Therapy (PDT) applications [21–23].

In recent years, PDT is becoming an important clinically approved treatment for various pathologies such as skin and infectious diseases, autoimmune disorders, and several tumors [24–26].

During PDT treatments, PS is so photo-activated by light irradiation at an appropriate wavelength, then the PS excited state returns to its ground state reacting with environmental molecular oxygen inducing the production of toxic Reactive Oxygen Species (ROS), such as H_2O_2, $^1O_2$, $^{\bullet}OH$ and $^{\bullet}O_2^-$ [24,25,27]. The generated ROS thus can explicate the photodynamic action causing the death of pathogen cells through apoptosis, necrosis or autophagia [28–30].

PBI derivatives employment as PSs for PDT is widely desirable due to their low dark toxicity [16,31] and their ability to absorb light in the photo-therapeutic range, the so-called *PDT window*, in the wavelengths range corresponding between the red and the near infrared region [31], since it penetrates deeper into living tissues.

However, one of the main drawbacks of these dyes are their very low solubility in biological media (aqueous solutions) and their low selectivity towards unhealthy cells. To overcome these limitations and to enhance the therapeutic effect of the PBI derivatives, the perylene bisimide can be functionalized either in the imide position or in the core with different groups that can increase their hydrophilicity and selectivity toward specific biological targets [31,32].

Furthermore, the elaboration of delivery systems capable to transport photosensitizers preferentially toward target sites [33] and the design of medical devices for direct localized treatments [34] are recently developing in biological and medical fields.

In this work, we propose a solid PBI-based thin film, as a medical device for possible therapeutic applications. The film was obtained immobilizing multilayers of an amphiphilic-asymmetric PBI derivative, the 2-(2-methoxyethoxy)ethyl)-9-(tridecan-7-yl) perylene bisimide derivative, onto a solid support, by means of the Langmuir-Schaefer (LS) technique [35–37], that allows to fabricate monolayer and/or multilayer films with controllable architecture, morphology, and preferential molecular orientations. In addition, the asymmetry of the side chains of this dye was also exploited to prompt peculiar aggregation and stacking phenomena among deposited molecules permitting to reach the final goal, that is singlet oxygen generation. We have prepared and tested different PBI concentrations for the preparation of the LS films and the different behaviors were analyzed, by varying the number of PBI layers to investigate the aggregation state of the PS within the film and to determine the most active film.

Then, the most performing PBI LS film was used to achieve measurements on human gynecological cancer C13 cell line. First, total absence of toxicity in the dark was demonstrated, subsequently the film was irradiated to induce the singlet oxygen production and cell killing.

The advantage of the LS technique for the preparation of photoactive devices is mainly related to the possibility to control the molecular organization within the film, a key factor for the photo-activation process [38]. Moreover, it is worth mentioning that the LS approach is a versatile method that guarantees the deposition of the compound of interest onto different kinds of solid supports, opening an important scenario in this case. PBI derivative could be deposited in the desired aggregation state onto biomedical support, such as plasters, or directly on the end of an optical fiber to reach inner tissues, even during a surgery.

2. Experimental section

2.1. Materials

The chemical structure of the amphiphilic and asymmetric PBI derivative, (2-(2-methoxyethoxy)ethyl)-9-(tridecan-7-yl) perylene bisimide derivative, ($C_{42}H_{48}N_2O_6$; FW: 676.8403) is reported in Fig. 1 (General Synthetic Scheme and Experimental Procedure are described in Supplementary Information). 1-Hexylheptylamine was synthesized following a reported method [39,40].

Uric acid (UA), chloroform (HPLC grade, ≥99.9%), hexamethyldisilazane (purity ≥ 99%), quartz slides (solid substrates), Roswell Park Memorial Institute (RPMI)-1640, trypsin, L-glutamine, penicillin–streptomycin (pen–strep), Fetal Bovine Serum (FBS), MTT (3-(4,5-dimethylthiazol-2-yl)-2,5-diphenol tetrazolium bromide), dimethyl formamide (DMF), 1,8-diazabicycloundec-7-ene, 1-butanol, 1-butyl bromide, dichloromethane, sodium sulfate, HCl, CH_3CN, methanol, glacial acetic acid, sulfuric acid zinc acetate dihydrate and 2-(2-Aminoethoxy)ethanol were purchased from Sigma-Aldrich. D_2O (99.96% of D) was purchased from VWR Chemicals. The water used in this work was purified from a Millipore Milli-Q system (18.2 MΩ cm).

2.2. Methods

The PBI derivative was dissolved in chloroform and solutions, at different concentrations, were characterized to study the possible formation of aggregate states. UV–Vis absorption spectroscopy was performed by means of a Varian Cary 5000 UV–Vis-NIR Spectrophotometer (Agilent) and a Fluorolog Jobin Yvon (Horiba) instrument, equipped with a NIR-sensitive liquid nitrogen cooled photomultiplier, was used to record fluorescence spectra.

The Langmuir curves were obtained by means of a NIMA 650 Langmuir trough spreading drop by drop 180 μL of chloroform

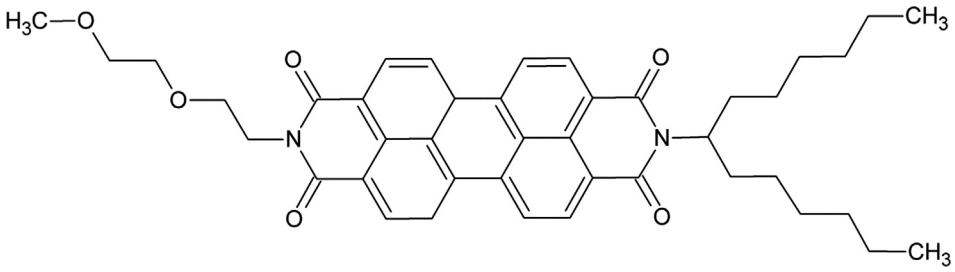

Fig. 1. Chemical structure of PBI derivative.

solution of the PBI derivative (at concentrations of 4.2×10^{-5} M and 1.5×10^{-4} M) onto a Milli-Q water subphase, at room temperature.

After chloroform evaporation, the floating layer was compressed using a constant barrier speed of 5 mm/min, and the surface pressure (Π) was recorded as a function of Area per molecule (Å^2/molecule) during the barrier motion.

The floating layer was further investigated by means of UV–Vis Reflection Spectroscopy (RefSpec) and Brewster Angle Microscopy (BAM) using the NIMA 650 Langmuir trough and a NFT BAM2plus system with a lateral resolution of 2 μm.

Then, the floating film was transferred onto hydrophobic quartz substrates by means of the Langmuir Schaefer (LS) deposition method [41], at a surface pressure of 16 mN/m. LS films with different numbers of PBI layers were prepared and UV–Vis spectroscopy, quartz crystal microbalance (QCM) measurements, Polarization-Modulation Infrared Reflection-Absorption Spectroscopy (PM-IRRAS), Steady State Fluorescence Spectroscopy and FTIR-ATR spectroscopy measurements [42] were performed to evaluate the arrangement of the PBI molecules on the solid support.

The Langmuir-Schaefer transfer process was monitored by means of an openQCM device (Novatech S.r.l.) [43]. An AT-cut quartz crystal (with a resonant frequency of 10 MHz) was used as a microbalance (frequency standard deviation of 0.4 Hz). The frequency variation measurements after each LS run were repeated on three different quartz crystal microbalances (QCMs) and averaged.

PM-IRRAS investigations were carried out by means of a KSV NIMA instrument and FTIR-ATR spectroscopy was carried out in Attenuated Total Reflection (ATR) mode by means a FTIR Spectrum One (PerkinElmer) instrument. In Figure S1 of the Supplementary Information, a photograph of a PBI LS film obtained with 15 layers of PBI at concentration of 1.5×10^{-4} M on quartz substrate is showed.

The ability of the PBI LS films to produce singlet oxygen after photo-excitation was performed by means of an indirect method, the uric acid (UA) test [27,44,45], and a direct method, the steady-state emission of $^1O_2$ in the NIR region [46].

The UA measurements were performed placing the PBI LS films on the bottom of a vial filled with 2 mL of uric acid solution at concentration of 10^{-4} M in phosphate buffer (KH_2PO_4/K_2HPO_4, 10^{-2} M, pH 7.5). Then, to induce the photo-activation of PBI, the system was irradiated by a LOT-Oriel Solar S class A (100 mW cm^{-2} light intensity) halogen lamp maintaining a constant distance (about 10 cm) between the lamp and the samples. The concentration of UA, in the supernatant solution, was analyzed by UV–Vis absorption spectra in the 250–600 nm range. Since this test is based on the fast reaction between UA and $^1O_2$ with the formation of allantoin [25,46], the decrease of the UA absorption intensity in buffer solution, at 290 nm, was continuously monitored for two hours and the values of UA absorption were recorded every 15 min.

In the case of direct detection of $^1O_2$, the PBI LS films were placed in a quartz cuvette at 45° with respect to the excitation beam. The cuvette was filled with 2 mL of D_2O and the system was irradiated with both a laser at 532 nm (50 mW) and the fluorimeter lamp set at the same wavelength. The use of D_2O as solvent for luminescence measurements evidences the advantage of the larger radiative constant and longer lifetime than in the case of H_2O. The measurements were performed using a Fluorolog-2 (Model, F111) spectrofluorimeter equipped with a NIR-sensitive liquid nitrogen cooled photomultiplier. The steady-state emission of $^1O_2$ was registered every 5 nm from 1220 to 1370 nm (slit: 58.8 nm, integration time: 2 s, 1 scan).

2.3. Cells lines and cell viability measurements

C13 (cervical cancer cells) were maintained in RPMI-1640 medium supplemented with 10% FBS, 2 mM glutamine, 100 U/ml penicillin and 10 mg/ml streptomycin. Cells were grown in a 5% CO_2 incubator at 37 °C. C13 cells were a kind gift of Dr. G. Marverti, University of Modena and Reggio Emilia.

Cell viability was assayed by MTT (3-(4,5-dimethylthiazol-2-yl)-2,5-diphenol tetrazolium bromide). Briefly, the PBI LS films were transferred in 12-well plate and C13 cells were seeded at a density of 2.0×10^5 cells/well and incubated for 24, 48 and 72 h to evaluate toxicity in the dark.

To analyze the phototoxic activity of PBI, cells were seeded as before and, after 24 h incubation, exposed to light for 30 min and 2 h. Measurements of toxicity were performed using a lamp emitting white light (400–700 nm) with a power surface density of 50 mW/cm^2.

Then, the medium was changed and after 24 h, 2 mL of MTT stock solution (5 mg mL^{-1} in PBS) were added to each well and cells were cultured for further 4 h. Subsequently, the formazan blue crystal was dissolved by replacing the medium with 2 mL of DMSO. The absorbance of the solutions was measured at 570 nm using a microplate reader Multilabel Plate Reader (Victor X5, PerkinElmer, USA). Conversion of MTT by mitochondrial succinate dehydrogenase was used as an indicator of cell viability [47,48].

No temperature variation was recorded under lamp irradiation in the experimental setup used for cell viability assay.

3. Results and discussion

3.1. Absorption and fluorescence measurements of PBI derivative solutions

PBI solutions in chloroform, in the concentration range between 7.0×10^{-6} to 4.2×10^{-5} M, were analyzed by means of UV–Vis absorption and fluorescence spectroscopy. It was not possible to show spectra of the most concentrated solutions due to detector saturation.

As reported in Fig. 2A, the steady-state UV–Vis absorption spectra exhibit the typical spectral features of perylene bisimide derivatives with two main absorption peaks at 527 nm and

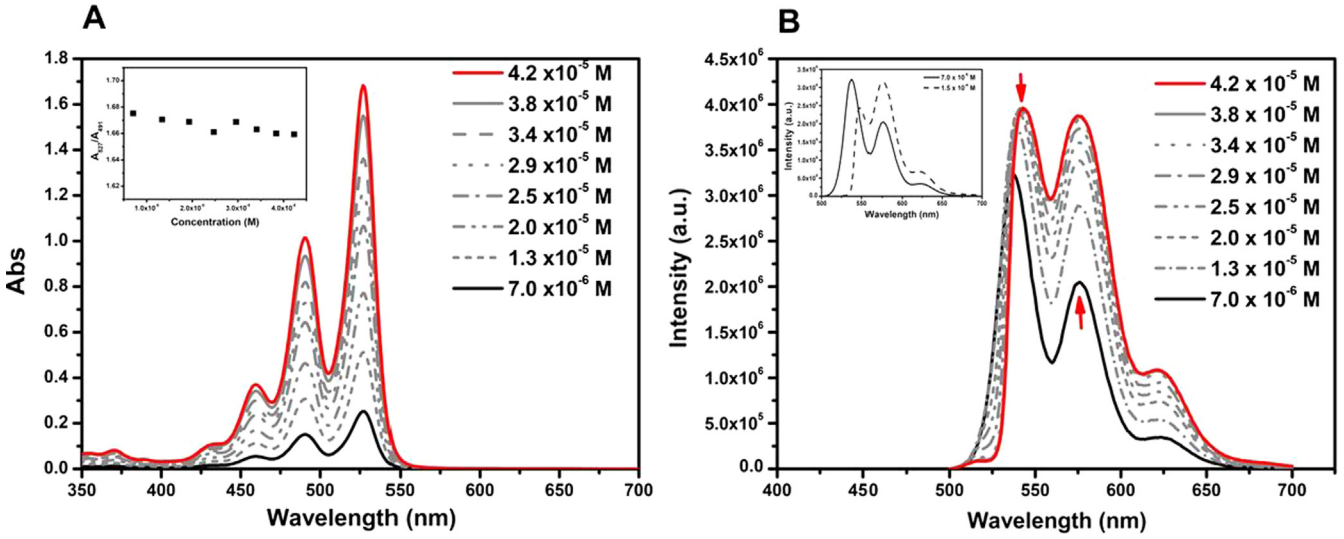

Fig. 2. Steady-state spectroscopic measurements of PBI in chloroform, from 7.0×10^{-6} to 4.2×10^{-5} M. (A) Absorption spectra at increasing concentrations. Inset: concentration-dependent absorption ratio ($A_{0\rightarrow0}/A_{0\rightarrow1}$) trend. (B) Emission spectra at increasing concentrations. Inset: Fluorescence spectra comparison between solutions at 7.0×10^{-6} and 1.5×10^{-4} M concentrations.

491 nm, corresponding respectively to the $0 \rightarrow 0$ and the $0 \rightarrow 1$ vibronic band of $S_0 \rightarrow S_1$ transitions and characterized by the ratio $A_{0\rightarrow0}/A_{0\rightarrow1}$ [2] equal to about 1.6 (Fig. 2A inset) [1,49,50]. This value undergoes small variations by increasing the concentration from 7.0×10^{-6} M to 4.2×10^{-5} M. At higher concentrations the increase of the $0 \rightarrow 0$ transition at 527 nm was more pronounced than the high-energy $0 \rightarrow 1$ band at 491 nm indicating a weakly aggregated state (Fig. 2A) [51].

The presence of molecular aggregates in more concentrated solution was also pointed out by steady-state fluorescence measurements, showed in Fig. 2B. At diluted concentrations, the emission spectra of the PBI are mirror images of the absorption spectra with two main emission peaks respectively at 538 nm and 576 nm. However, regular changes in the fluorescence spectra of PBI were observed as the concentration was increased. It is possible to note a gradual bathochromic shift of the higher emission peak, and a gradual change in the ratio of the intensity of the two main emission peaks up to a total inversion of the two peaks intensities at concentration of 1.5×10^{-4} M, as shown in the inset of Fig. 2B. Indeed, the spectrum of this solution presents a light hypochromic effect of the 576 nm emission peak, typically reported in the case of formation of supramolecular aggregates [2]. This behavior is characteristic of PDI excimer formation [3,52]. Furthermore, the spectra of higher concentrated solutions are characterized by a broad and structure-less emission, which is a typical feature of the PBI aggregate emission spectra [53].

These measurements suggest that, in the cases of higher concentrations, there is the coexistence of monomeric and aggregate states. Numerous studies regarding the self-assembly of PBIs derivatives reported that, in solution, the aggregation process of PBIs can be considered as the result of an equilibrium between monomeric and aggregate species [1,51,54].

3.2. Time resolved fluorescence spectroscopy

The fluorescence decay of three PBI solutions in chloroform at different molar concentrations (7.0×10^{-6}, 4.2×10^{-5}, and 1.5×10^{-4} M) was investigated upon 455 nm excitation. Table 1 reports the decay constants (τ, ns), the relative amplitude factors (%), the χ^2 parameter for each fluorescence decays fittings and the emission wavelengths. Moreover, the fluorescence decay spectrum and the residue distribution, obtained respectively for each PBI solution, are reported in Figs S2, S3 and S4 of the Supplementary Information. The measurements show that the lifetime values increased with increasing in concentrations.

The fluorescence decay profiles of the two most diluted solutions were fitted by mono-exponential functions; comparable decay times of 3.41 and 4.06 ns for the solution at 7.0×10^{-6} and 4.2×10^{-5} M, respectively, were found. This lifetime could be imputable to the monomeric form of the compound according to the literature [55]. Nonetheless, a small increase of the lifetime in the 4.2×10^{-5} M solution could be ascribable to some (even small) aggregation phenomena, according to the previous spectroscopic characterization. Authors reported that the increasing of fluorescence lifetime is due to the reduced transition probability of an S_1 to S_0 transition commonly observed in H type aggregates [1]. This was also evidenced by recording a bathochromic shift in the steady state fluorescence spectrum (Fig. 2B).

The fluorescence decay of the 1.5×10^{-4} M solution, instead, was fitted by a bi-exponential function, and two lifetimes were monitored. The longer one (4.58 ns), characterized by the higher relative amplitude of about 70% and by a further increase, should be due to more pronounced aggregation phenomena, in agreement with the partial formation of excimer state [3], according again to the recorded red shift in the relative fluorescence spectrum

Table 1
Decay profiles of PBI solutions at different concentrations.

Concentration (M)	τ_1 (ns)	Amplitude (%)	τ_2 (ns)	Amplitude (%)	χ^2	λ_{em} (nm)
7.0×10^{-6}	3.41	100	–	–	1.32	520
4.2×10^{-5}	4.06	100	–	–	1.59	550
1.5×10^{-4}	4.52	70.49	0.62	29.51	1.41	590

(Fig. 2B). The shorter lifetime of 0.62 ns further confirmed the strong aggregation characterizing the PBI at this concentration. In fact, this can be attributed to very fast non-radiative decay processes already reported in presence of PBI aggregates in aqueous media [56].

However, despite the PBI solution at lower concentration does not present aggregate forms, it is very diluted to form appreciable floating film at the air/water interface to be then deposited onto solid supports. Consequently, with this aim, the 4.2×10^{-5} and 1.5×10^{-4} M solutions were chosen and utilized to fabricate LS films; the molecular arrangements and photo-responsivity of PBI-based films were so studied.

3.3. Characterization at the air/water interface

The two PBI chloroform solutions at concentrations of 4.2×10^{-5} M and 1.5×10^{-4} M were spread at the air-Milli-Q water interface and characterized by means of different techniques.

In Fig. 3 are reported the Surface Pressure Π (mN/m) vs Area per Molecule (Å^2/mol) curves.

For both solutions, the Π-Area isotherms showed initial long pseudo-gaseous phases which indicate small interactions between the PBI molecules spread on the subphase, followed by a rise of surface pressure at about 300 Å^2/mol for the solution at 4.2×10^{-5} M concentration, and about 86 Å^2/mol for the solution at 1.5×10^{-4} M concentration. The values of limiting area per repeat unit were about 200 Å^2/mol and 65 Å^2/mol, respectively. Considering that the average area occupied by the rigid skeleton of perylene is about 104 Å^2 [57], the limiting area value found for the lower concentration (200 Å^2/mol) evidences a lack of aggregation upon barriers motion and the presence of uncovered portions of the water subphase. Instead the value of limiting area calculated in the case of the higher concentration (86 Å^2/mol) suggests the presence of aggregates at the air-liquid interface. Moreover, the rigid cores of PBI cannot be supposed totally prone onto the water surface but slightly tilted, as already reported in the literature for other perylene derivatives LS films [57,58] and other compounds such as porphyrins [59]. In this configuration, it is possible to suppose that the aromatic cores are densely π-π packed into tubular aggregates almost parallel to the water surface whereas the flexible hydrophobic chains are directed towards air. The collapse point appears more evident in this curve (Fig. 3B) supporting the formation of a dense molecular packing with greater rigidity if compared with the floating layer obtained with the lower PBI concentration. The limiting area value found in this case, 200 Å^2/mol, evidences instead a reduced aggregation upon barriers motion, due also to uncovered portions of the water subphase.

The molecular organization of PBI floating layers at the air/water interface was also investigated by means of Reflection Spectroscopy measurements (RefSpec). Since the reflection variations of light under normal incidence between the PBI floating layer on the subphase and the bare subphase surface have been demonstrated to be proportional to the absorbance of the floating layer, it is possible to consider the reflection spectra as absorption spectra [36,60]. The reflection profiles of the PBI floating layers on water subphase were registered at low surface pressure (Π = 2 mN/m) and at the deposition surface pressure (Π = 16 mN/m), using the two PBI solutions at concentrations of 4.2×10^{-5} M and 1.5×10^{-4} M (Fig. 4). All the spectra reported in Fig. 4 highlight the presence of a more intense peak, which corresponds to the 0 → 0 vibronic band, at about 498 nm, and another less intense peak corresponding to the 0 → 1 vibronic band, at about 476 nm. These peaks exhibit blue shifts, decrease in the absorbance peaks

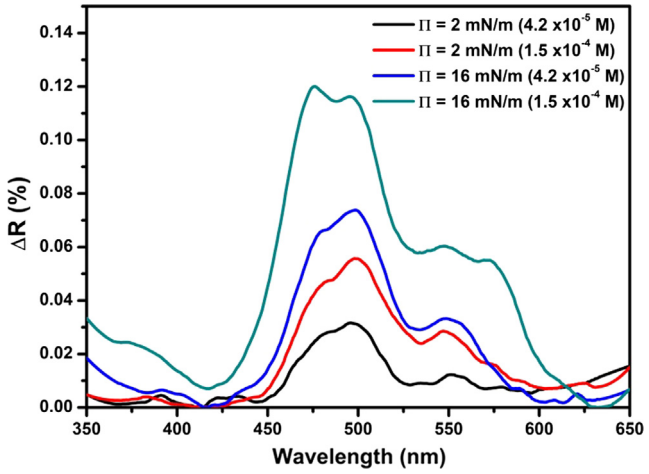

Fig. 4. Reflection spectra of floating layers of PBI at 4.2×10^{-5} M and 1.5×10^{-4} M concentrations on ultrapure water subphase registered at two surface pressures Π (2 mN/m and 16 mN/m).

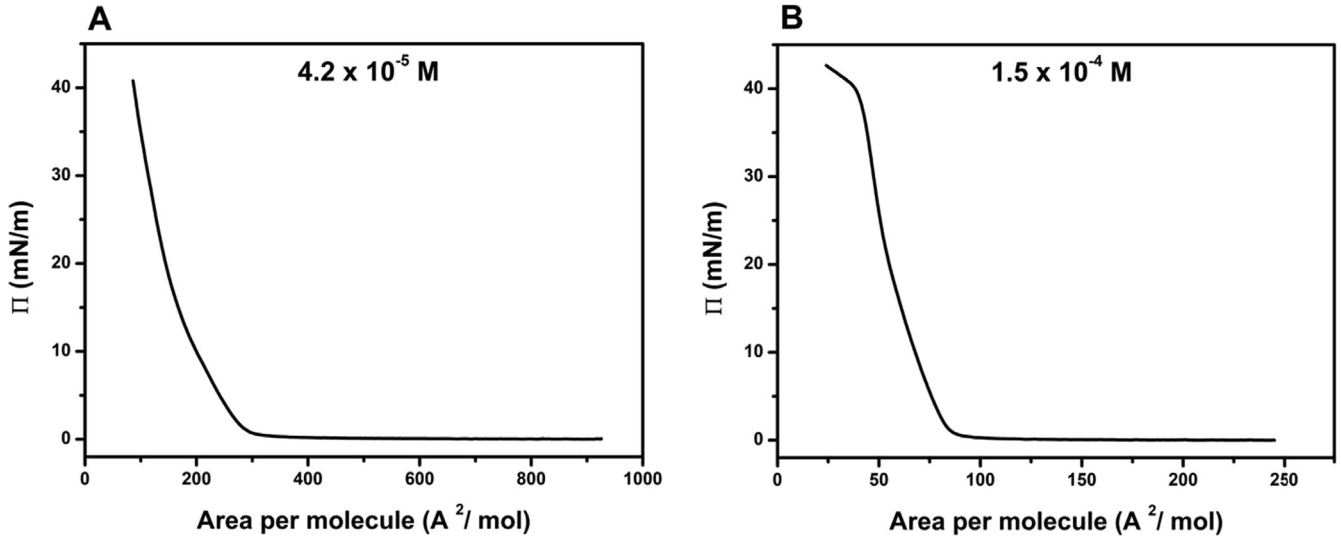

Fig. 3. Π-Area curves of the floating layers of PBI at 4.2×10^{-5} M (A) and 1.5×10^{-4} M (B) at the air/water interface.

$A_{0\to0}/A_{0\to1}$ ratio and broadening of the bands if compared to the absorption spectra registered in chloroform solution (Fig. 2A). These behaviors are indicative of self-aggregates formation of PBI molecules [57] at the air/water interface.

The floating layers reflection spectra registered at deposition surface pressure of 16 mN/m, for both concentrations, showed a clear enhancement of the absolute reflection due to the increase of the molecular surface density. However, in the case of the most concentrated solution (1.5×10^{-4} M) the curve (Fig. 4, green line) revealed a considerable inversion of peaks intensities, suggesting the presence of PBI aggregates and a closer packing of molecules, according to the behavior of the Π -Area curve.

Hypsochromic effect and inversion of the principal peaks of absorption spectra might be related to the formation of π-π stacked aggregates, reported as H aggregates for similar systems [61] and for other Langmuir films of aromatic compounds [62].

Brewster Angle Microscopy (BAM) was performed to investigate the PBI floating films and the relative pictures are reported in Fig. 5. BAM is a technique utilized to monitor directly the morphology of floating layers at the air/water interface during the motion of the barriers. Indeed, the BAM images give information about thickness and roughness of floating layers and the presence of three-dimensional aggregates. The floating layer obtained by spreading the lower concentration of PBI, after the solvent evaporation, is

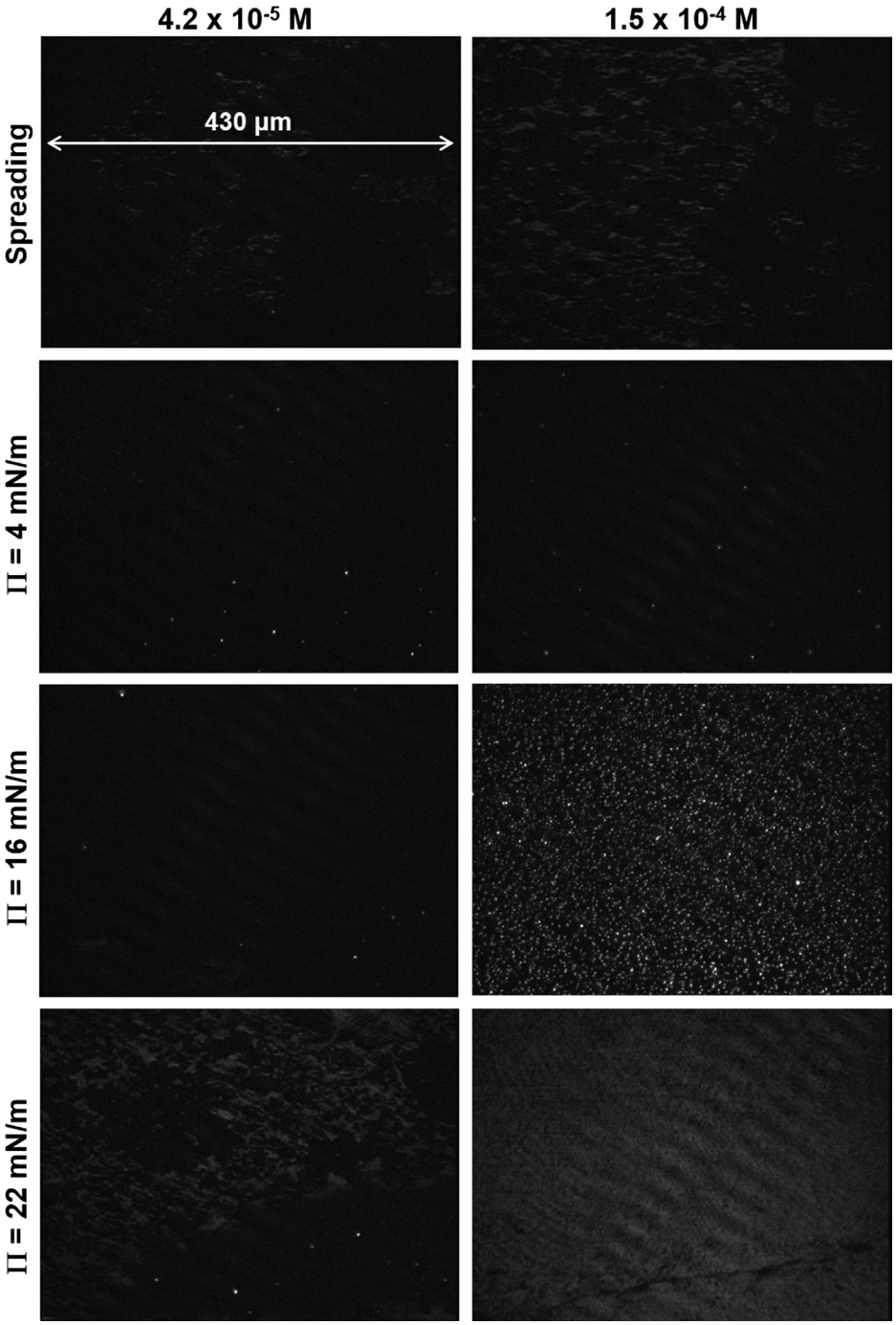

Fig. 5. BAM images of floating layers of PBI 4.2×10^{-5} M (left strip) and 1.5×10^{-4} M (right strip) taken at different surface pressure.

characterized by the co-existence of uncovered areas of subphase and three-dimensional aggregates. Upon barrier motion, at low surface pressure values, the layer appears constituted by a very thin homogenous floating layer and by the presence of small and few brilliant 3D aggregates. By increasing the surface pressure up to 16 mN/m, such a thin layer becomes lighter in accordance with the increased thickness and to reflection spectroscopy investigations. At high pressure values, the 3D aggregates strongly increase both in number and dimension. In the other case, when the higher concentration of PBI was spread onto water subphase, the presence of coalescent domains, particularly larger and denser than in the case of 4.2×10^{-5} M concentration, is clear. During compression of the floating layer, there is a gradual increase in both the thickness of the film and the number of bright domains up to 16 mN/m where the density of the 3D bright aggregates is very significant. Finally, at high surface pressure values, according to the Langmuir curve, the floating layer presents a dense molecular packing with irregular multilayers.

3.4. Characterization of PBI LS films

To study the molecular organization of PBI onto solid supports, UV–Vis absorption and fluorescence measurements were performed and the relative spectra are showed in Fig. 6. The films were realized transferring 5, 10 and 15 floating layers of PBI, at starting concentrations of 4.2×10^{-5} M and 1.5×10^{-4} M, onto quartz substrates by the LS technique. The absorption spectra of PBI LS films (Fig. 6A and C) preserve almost completely the shape of the spectra of PBI floating layers at the same concentration (Fig. 4). The two main bands, corresponding to the $0 \rightarrow 0$ and $0 \rightarrow 1$ vibronic bands, present indeed blue shifts and changes of the absorption peaks ratio in comparison to the spectra of PBI in chloroform solution. These behaviors confirm the presence of partial aggregative phenomena among PBI molecules also within the LS films. Moreover, in the case of the LS film obtained with the higher concentration of PBI, a considerable inversion of the absorption peaks was again observed (Fig. 6C) confirming the presence of more aggregates and of a denser packing of PBI molecules within the film. It was also demonstrated that by increasing the PBI concentration, aggregation phenomena raise as well. These results further confirm the rationale from the RefSpec investigations, i.e. that the deposition technique retains in both cases onto solid substrates the molecular organization already observed at the air–water interface. It is worth noting that for both concentrations, the maximum absorption intensity located at 497 nm and 467 nm, respectively, linearly increased with the number of layers, indicating the reproducibility of the deposition process [63] up to at least 15 LS runs (inset in Fig. 6A and C). According to these evidences, the

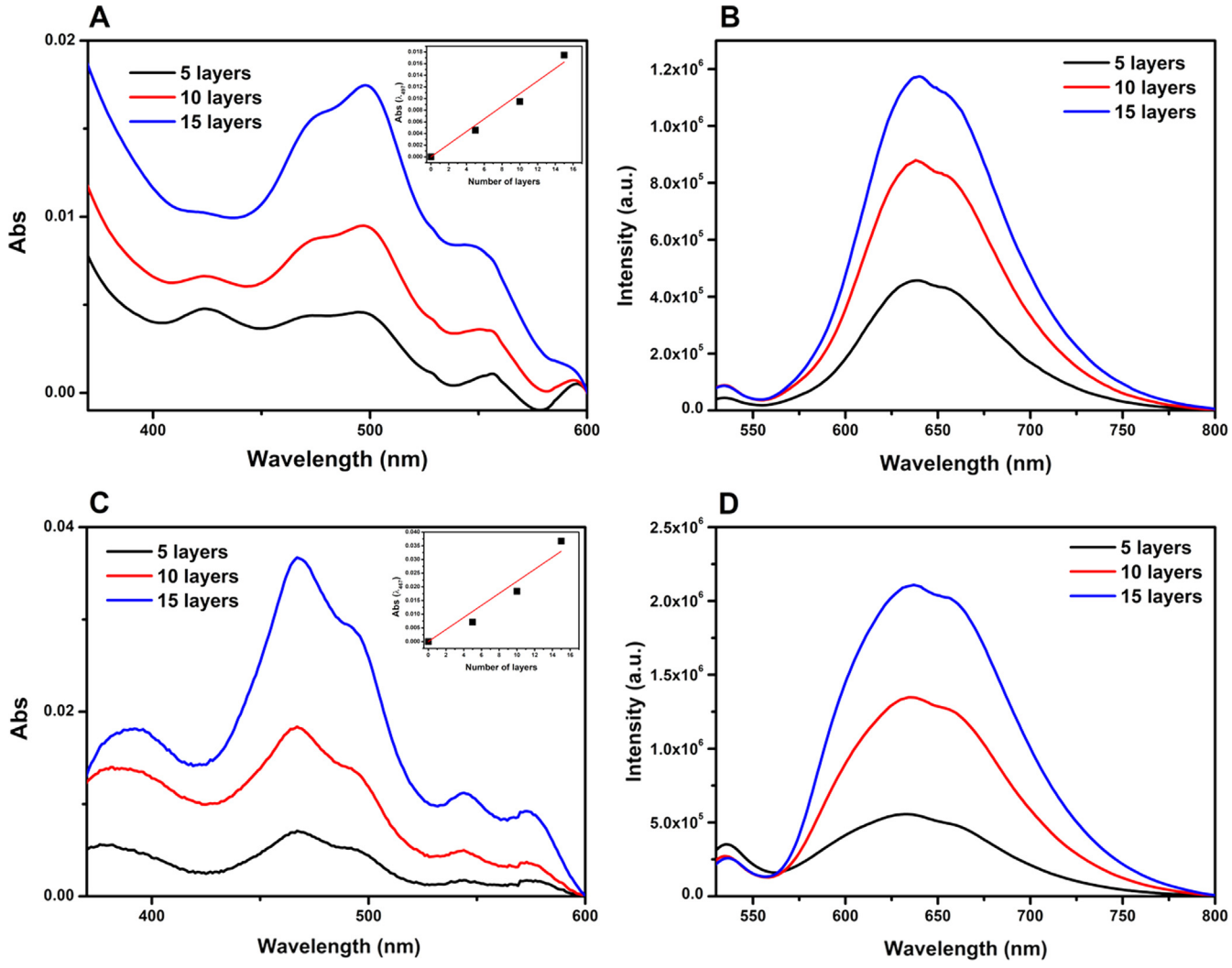

Fig. 6. UV–Vis adsorption spectra of PBI LS films with 5, 10 and 15 layers of PBI at concentration of 4.2×10^{-5} M (A) and 1.5×10^{-4} M (C) on quartz substrate. In the inset are reported the maximum adsorption vs the number of layers. Fluorescence spectra of PBI LS films with 5, 10 and 15 layers of PBI at concentration of 4.2×10^{-5} M (B) and 1.5×10^{-4} M (D) on quartz substrate.

fluorescence intensity of the films improved by increasing the PBI layer number (Fig. 6B and D). This behavior can be rationalized also considering that the deposition process ensured the absence of self-absorption of PBI [53].

A very high reproducibility of the transfer process in the case of 1.5×10^{-4} M and of 4.2×10^{-5} spreading solution was also confirmed by quartz crystal microbalance (QCM) measurements. In fact, the linear relation between the resonant frequency variation of the quartz crystal microbalance and the number of LS layers transferred (Fig S5 of Supplementary Information) suggests that the same amount of active molecules are transferred from the floating film to the solid support at each LS run. In agreement with the Sauerbrey equation [64], the resonant frequency of a piezoelectric transductor is directly proportional to the mass present on the resonator [42,65,66], so it can be concluded that the deposition method adopted appears particularly suitable for the PBI derivatives here used.

Furthermore, frequency variation induced on the microbalance when 15 LS runs were transferred on the QCM support by spreading 180 μL of 4.2×10^{-5} M and 1.5×10^{-4} M are 984 Hz and 896 Hz, respectively. These two values appear very similar, suggesting that a comparable amount of perylene molecules are transferred in the two cases.

In order to better understand the organization of the PBI within the LS films, FT-IR spectroscopy and PM-IRRAS characterizations were carried out. PM-IRRAS, in fact, is a powerful technique to predict the spatial disposition of a chemical group at an interface [67]. Fig. 7A reports PM-IRRAS spectra of PBI LS films obtained with 15 LS layers of the less concentrated starting solution of PBI (grey line) and the more concentrated one (black line), in the 1750–1000 cm^{-1} range. The spectrum of a PBI chloroform solution casted directly on the ATR plate is depicted too (green line, Fig. 7B) to make easier peaks attribution. The green spectrum is dominated by the signals comprised between 1720 and 1640 cm^{-1} which are assigned to imidic C=O stretching modes; then the signals typical of aromatic compounds are visible in the 1600–1560 cm^{-1} range (C=C stretching modes). The signals located at about 1399, 1344, 1248, 1177, 1125 and 1160 cm^{-1} can be mainly attributed to CH_3 (asymmetric and symmetric stretching) and CH_2 (scissoring) vibrations, tertiary and amidic CN stretching and C—O stretching modes respectively [68]. By observing the PM-IRRAS spectra reported in Fig. 7A for the two different films, it is possible to claim that, in both cases, a preferential organization on the solid support is induced. In the film obtained with the more concentrated solution, the PBI molecules could assume a partial prone conformation on the solid support, with the aromatic core just slightly tilted; in fact, the contribution at 1593 cm^{-1} in the case of the black line almost disappears, as indicated by the red arrow. Instead, the two flexible chains vibrations C—N modes and both C=O modes are still visible, indicating that the chains are not-parallel to the substrate. On the other hand, the situation resulted different for the other film (grey line, Fig. 7A). In fact, the PBI moieties appear vertically oriented with respect to the substrate surface. The aromatic C=C mode is well visible (black arrow, Fig. 7A) as well as the C=O, C—N and even the C—H modes. In this case, an edge-on organization of the PBI aromatic core upon barrier motions could be hypothesized. These results are in very good agreement with both Langmuir through experiments and UV–Vis and Fluorescence spectroscopy characterization. In fact, by changing the starting concentration of PBI solution, the aggregate number and size within the LS film obtained onto the solid support can be tuned and consequently the optical properties of the PBI films as well.

3.5. Singlet oxygen production

Energy transfer from the excited state of PBI molecules, deposited onto solid supports, to molecular oxygen present in the system inducing the production of $^1O_2$ was assessed by uric acid (UA) test and by near-infrared luminescence investigations. Fig. 8 reports on the normalized absorbance intensity at 290 nm versus the illumination time of UA in buffer solution in presence of PBI LS film upon solar simulator (100 mV/cm^2) irradiation. The decreasing of UA absorbance values, due to the reaction between UA and $^1O_2$ with a consequent formation of allantoin [25], was showed. In Fig. 8A the effect of the two PBI LS films obtained with 15 layers of PBI from 1.5×10^{-4} M (black squares) and 4.2×10^{-5} M spreading solution concentrations (red squares) have been compared. The 15 LS runs film prepared with the less concentrated PBI starting solution showed a greater efficiency in the $^1O_2$ production than the LS film prepared with the same number of layers from PBI spreading solution at higher concentration. In fact, an almost 70% reduction of the UA maximum absorption could be monitored in

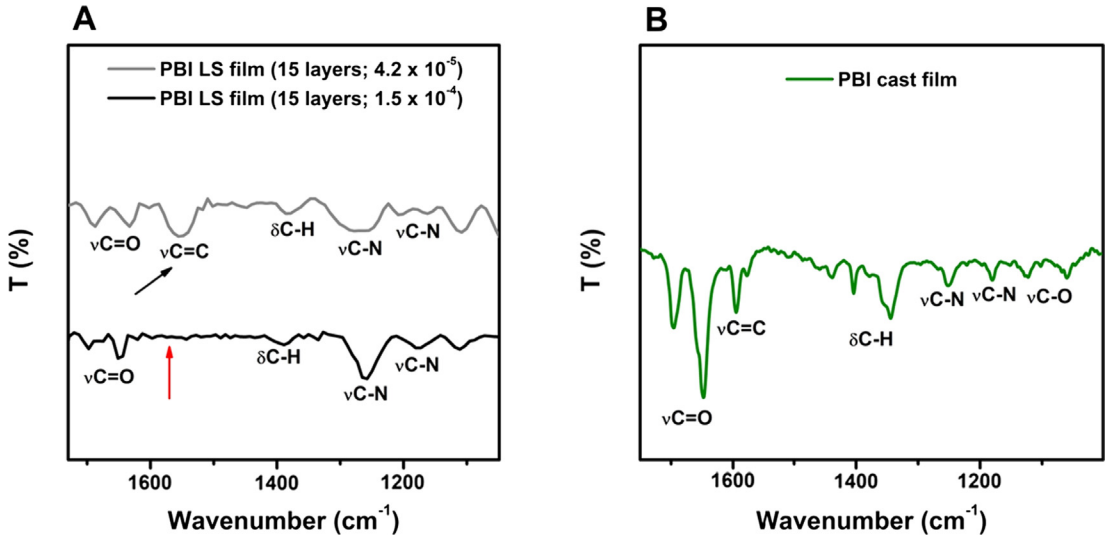

Fig. 7. PM-IRRAS spectra of PBI LS films (15 layers) obtained with PBI solutions at initial concentrations of 4.2×10^{-5} and 1.5×10^{-4} M (grey and black lines, respectively) compared to FT-IR spectrum of PBI solution (green line) in the range 1750–1000 cm^{-1} (A) and 1730–1560 cm^{-1} (B). (For interpretation of the references to colour in this figure legend, the reader is referred to the web version of this article.)

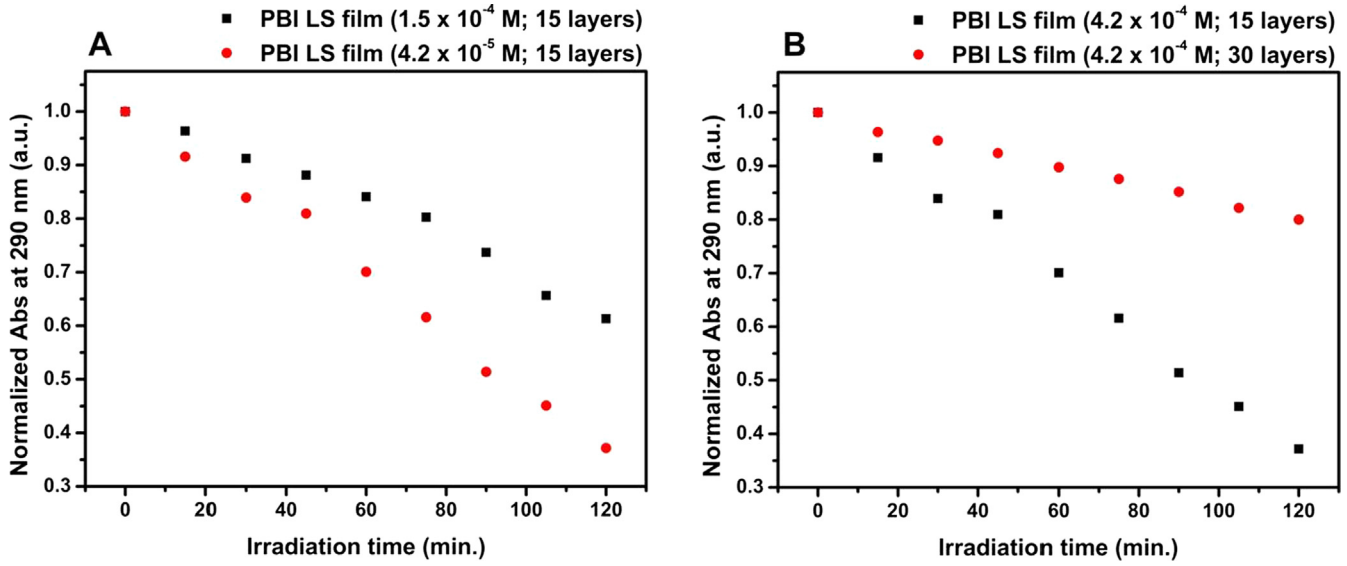

Fig. 8. Time decrease of normalized absorption peak at 290 nm of UA 10^{-4} M in buffer solution in the presence of PBI LS films under illumination. (A) PBI LS films obtained with 15 layers of PBI at initial concentration of 1.5×10^{-4} M and 4.2×10^{-5} M, respectively. (B) PBI LS films obtained with 15 and 30 layers of PBI at initial concentration of 4.2×10^{-5} M.

the first case, whilst the second film induced a reduction of just 40%. These results are in good agreement with the previous characterization of both films. When a 1.5×10^{-4} M concentration of PBI solution was used, a strong aggregated PBI molecules organization within the LS film was observed and thus, despite a quite high fluorescence emission intensity was preserved (Fig. 6D), a reduction of the photo-production of singlet oxygen was induced. The edge-on configuration of the PBI aromatic core, in the case of the 4.2×10^{-5} M concentration, clearly avoided random aggregation phenomena, ensuring singlet oxygen production with good efficiency [15].

Furthermore, it was verified whether an additional increase of PBI layers could improve the efficiency of the system obtained using the less concentrated PBI solution (4.2×10^{-5} M). The values of UA absorption intensity in the presence of 15- and 30-layered PBI films (black squares and red circles, respectively), during the illumination time, are reported in Fig. 8B. The measurement clearly evidences that by transferring thicker films than 15 layers, a loss in photo-responsiveness has been recorded, due to a reduced reproducibility of the deposition process, according to self-aggregation phenomena within a layer and aggregation phenomena between different layers. Moreover, the UV–Vis adsorption spectra of PBI LS films made by 15 layers of PBI at 4.2×10^{-5} M and 1.5×10^{-4} M were also recorded before and after 2 h of illumination to investigate the photochemical stability of the photosensitizer in the experimental conditions used. These measurements, shown in Fig S6 of Supplementary Information, allow to verify a high photo-stability and no dye degradation upon illumination.

The production of $^1O_2$ by the PBI LS films made up by 15 and 30 layers of PBI at a starting concentration of 4.2×10^{-5} M was also tested by near-infrared luminescence spectroscopy. The typical luminescence of this transient species, in the NIR region, was measured after photo-excitation. Fig. 9 shows a clearly visible signal of $^1O_2$ photo-generation from LS film with 15 layers of PBI, whereas the signal was not observable using this technique in the case of LS film with 30 layers of PBI (Fig S7 in Supplementary Information). These data are in very good agreement with the previous UA test measurements.

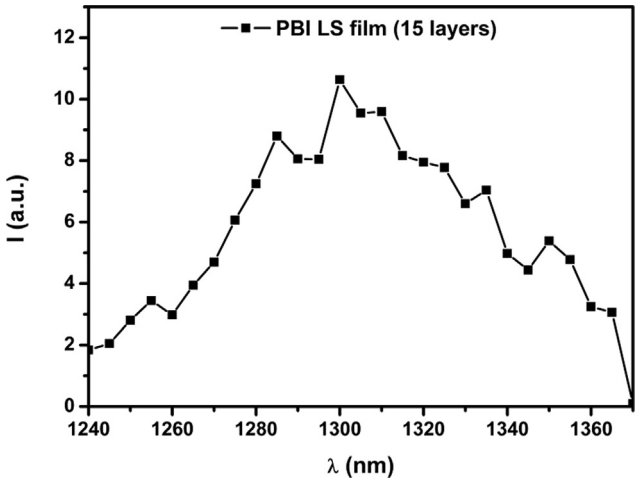

Fig. 9. Singlet oxygen luminescence of PBI LS films obtained with 15 layers of PBI at initial concentration of 4.2×10^{-5} M. The films were immersed in 2 mL of D_2O and irradiated with 532 nm laser excitation (50 mW).

3.6. Cytotoxicity and photo-cytotoxicity test

Due to its ability to generate $^1O_2$, the PBI LS film obtained with 15 layers of PBI at a starting concentration of 4.2×10^{-5} M was then tested onto human cervical carcinoma C13 cell line to propose it for Photodynamic Therapy (PDT) applications.

MTT assay was utilized to evaluate cytotoxicity of the PBI LS film in the absence or presence of light. The low toxicity in the dark of photosensitizer is the first prerequisite for successful cancer PDT [24]. Thus, the cells were seeded onto the PBI LS films and were incubated at different times (24, 48 and 72 h) to evaluate cells viability in dark conditions. As shown in Fig. 10A, C13 cells did grow in these conditions, doubling at 72 h compared to 24 h. These results demonstrated that PBI LS films did not affect cell viability in the dark. Then, we have tested if photo-activation of PS LS films determined alterations in cell viability. Cells were seeded onto the film

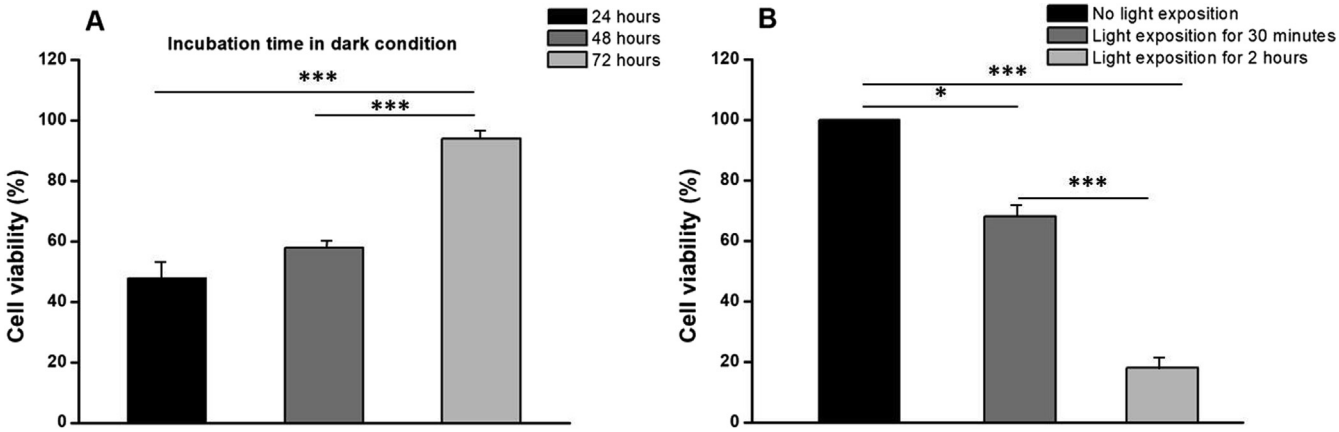

Fig. 10. Cell viability on C13 cell line determined by MTT assay. (A) Cells seeded on PBI LS films, incubated respectively 24, 48 and 72 h and maintained in dark conditions. (B) Cells seeded on PBI LS films incubated 24 h and irradiated for 30 min and 2 h. Data represent the mean ± s.e.m. of at least three independent experiments ($^{*}P \leq 0.05$ and $^{**}P \leq 0.01$ $^{***}P \leq 0.001$).

and after 24 h of incubation were exposed to white light for 30 min and 2 h, and cell viability was evaluated by means of MTT assay. As showed in Fig. 10B, a significant photo-toxicity for both illumination times was recorded compared to cells at t_0 (time zero), corresponding to the non-illuminated film and used as control.

These results suggest an interesting photo-toxicity of PBI LS film, resulting from generation of singlet oxygen under light irradiation that has been demonstrated to efficiently induce cancer cells death. Also, cell mortality increases with the illumination time, confirming the quality of the external trigger, i.e. light. For these reasons, this system could represent an excellent model device to understand the mechanism of cell death activated by singlet oxygen (and other eventual produced ROS) and for future studies on PDT.

4. Conclusions

The (2-(2-methoxyethoxy)ethyl)-9-(tridecan-7-yl) PBI derivative was previously characterized in solution to determine the appropriate conditions for its deposition onto quartz supports by means of Langmuir-Schaefer (LS) technique. Before deposition, the floating layers of PBI at 4.2×10^{-5} M and 1.5×10^{-4} M concentration were investigated at the air/water interface by Surface Pressure vs Area per Molecule curves, Reflection Spectroscopy and Brewster Angle Microscopy.

These three techniques have allowed to observe the presence of π-π aggregates within the floating layers which tend to grow as PBI concentration increases.

The same trend was proved by UV–Vis absorption and fluorescence measurements also in the case of solid LS films of PBI. Moreover, the PM-IRRAS characterization was performed to understand the spatial organization of the PBI molecules within the LS films. It is possible to note that, in the case of PBI LS films obtained with 15 PBI layers of the less concentrated solution, the PBI molecules appear to be vertically oriented with respect to the substrate surface with an edge on organization. On the contrary, in the PBI LS films obtained with the more concentrated solution, the PBI molecules could assume a partial prone conformation on the solid support. Their aromatic core can be hypothesized as little bit tilted forming several aggregates packed into 3D tubular arrangements.

Subsequently, singlet oxygen production by photo-excitation of PBI LS films was studied. Since it is known that the chemical environment, in which the chromophore is dispersed, plays a crucial role influencing the absorption features, in particular in biological systems, in this work all photo-excitation experiments were performed using a light source with a broad emission range.

The best efficiency in the $^1O_2$ production was observed for the PBI LS films made up by 15 layers of PBI at a starting concentration of 4.2×10^{-5} M. Then, this film was used to perform photo-toxicity tests onto human cervical carcinoma C13 cell line revealing absence of cytotoxicity in dark conditions and a high photo-cytotoxicity. Furthermore, the toxic effect was demonstrated to be dependent on the illumination time. Indeed, after 2 h of illumination cell viability was less than 20% due to cell damage induced by $^1O_2$.

In conclusion, the chemical physical characteristics of PBI LS films were systematically studied and non-toxicity in dark conditions but very remarkable photo-toxicity towards C13 cells were successfully demonstrated. The results suggest that the studied PBI LS film may be a promising candidate as photoactive device for PDT applications. In fact, this film can be considered as a reservoir of singlet oxygen precursor, able to release $^1O_2$ on demand, in situ and at controlled concentration upon illumination. The chosen trigger, the light, can be considered as a very elegant external trigger in biomedical applications due to the low cytotoxicity and the possibility to tune both the intensity and the time of exposition, allowing a high control on the release process. It is also very important to underline that the LS deposition technique is a very versatile approach which has even the advantage to require very low quantities of dye (a few hundred of microliters of very diluted solutions). In fact, by means of LS technique, it is possible to transfer the PBI on different supports, such as plasters, bandage, ointments or optical fibers to realize various medical devices. Besides, the realization of low-cost photodynamic therapy devices would allow the direct action of the photosensitizer *in loco* avoiding the use of drug delivery systems [24,69].

However, the influence of exciting wavelength and of the light intensity on different PBI derivatives, the photo-toxicity effect toward other cancer cell lines will be investigated in following studies. In fact, it will be interesting to investigate in the future the molecular mechanisms activated by this device and the potential of this technique comparing chemoresistant and chemosensitive cancer cells in order to establish its therapeutical power using both 2D- and 3D- cell culture.

Acknowledgment

This study was financed by the Fondazione "Banca Popolare Pugliese Giorgio Primiceri"-Onlus and also partially supported by AIRC (Associazione Italiana per la Ricerca sul Cancro), Investigator Grant 2016N. 19068 to C. B. MP is grateful to the Basque Foundation for Science (Ikerbasque), the AXA Research Fund, and the

Maria de Maeztu Units of Excellence Program from the Spanish State Research Agency – Grant No. MDM-2017–0720.

Appendix A. Supplementary data

Supplementary data to this article can be found online at https://doi.org/10.1016/j.jcis.2019.06.037.

References

[1] F. Wurthner, C.R. Saha-Moller, B. Fimmel, S. Ogi, P. Leowanawat, D. Schmidt, Perylene bisimide dye assemblies as archetype functional supramolecular materials, Chem. Rev. 116 (3) (2016) 962–1052.

[2] M. Burian, F. Rigodanza, H. Amenitsch, L. Almasy, I. Khalakhan, Z. Syrgiannis, M. Prato, Structural and optical properties of a perylene bisimide in aqueous media, Chem. Phys. Lett. 683 (2017) 454–458.

[3] E.A. Margulies, L.E. Shoer, S.W. Eaton, M.R. Wasielewski, Excimer formation in cofacial and slip-stacked perylene-3,4:9,10-bis(dicarboximide) dimers on a redox-inactive triptycene scaffold, PCCP 16 (43) (2014) 23735–23742.

[4] T.J. Tang, J. Qu, K. Mullen, S.E. Webber, Water-soluble perylene diimides: solution photophysics and layer-by-layer incorporation into polyelectrolyte films, Langmuir 22 (18) (2006) 7610–7616.

[5] X.J. Zhan, J. Zhang, S. Tang, Y.X. Lin, M. Zhao, J. Yang, H.L. Zhang, Q. Peng, G. Yu, Z. Li, Pyrene fused perylene diimides: synthesis, characterization and applications in organic field-effect transistors and optical limiting with high performance, Chem. Commun. 51 (33) (2015) 7156–7159.

[6] C. Huang, S. Barlow, S.R. Marder, Perylene-3,4,9,10-tetracarboxylic acid diimides: synthesis, physical properties, and use in organic electronics, J. Org. Chem. 76 (8) (2011) 2386–2407.

[7] M. Burian, F. Rigodanza, N. Demitri, L. Dordevic, S. Marchesan, T. Steinhartova, I. Letofsky-Papst, I. Khalakhan, E. Mourad, S.A. Freunberger, H. Amenitsch, M. Prato, Z. Syrgiannis, Inter-backbone charge transfer as prerequisite for long-range conductivity in perylene bisimide hydrogels, ACS Nano 12 (6) (2018) 5800–5806.

[8] E. Kozma, M. Catellani, Perylene diimides based materials for organic solar cells, Dyes Pigm. 98 (1) (2013) 160–179.

[9] C. Li, H. Wonneberger, Perylene imides for organic photovoltaics: yesterday today, and tomorrow, Adv. Mater. 24 (5) (2012) 613–636.

[10] A. Kalita, S. Hussain, A.H. Malik, N.V.V. Subbarao, P.K. Iyer, Vapor phase sensing of ammonia at the sub-ppm level using a perylene diimide thin film device, J. Mater. Chem. C 3 (41) (2015) 10767–10774.

[11] Y.B. Zhang, C. Peng, X.J. Ma, Y.K. Che, J.C. Zhao, Fluorescent and photoconductive nanoribbons as a dual-mode sensor for selective discrimination of alkyl amines versus aromatic amines, Chem. Commun. 51 (81) (2015) 15004–15007.

[12] M. Bouvet, H. Xiong, V. Parra, Molecular semiconductor-doped insulator (MSDI) heterojunctions: Oligothiophene/bisphtalocyanine (LuPc2) and perylene/bisphthalocyanine as new structures for gas sensing, Sens. Actuat. B-Chem. 145 (1) (2010) 501–506.

[13] J.C. Hu, W.F. Kuang, K. Deng, W.J. Zou, Y.W. Huang, Z.X. Wei, C.F.J. Faul, Self-assembled sugar-substituted perylene diimide nanostructures with homochirality and high gas sensitivity, Adv. Funct. Mater. 22 (19) (2012) 4149–4158.

[14] L. Rossetti, M. Franceschin, A. Bianco, G. Ortaggi, M. Savino, Perylene diimides with different side chains are selective in inducing different G-quadruplex DNA structures and in inhibiting telomerase, Bioorg. Med. Chem. Lett. 12 (18) (2002) 2527–2533.

[15] K.M. Lefler, K.E. Brown, W.A. Salamant, S.M. Dyar, K.E. Knowles, M.R. Wasielewski, Triplet state formation in photoexcited slip-stacked perylene-3,4:9,10-bis(dicarboximide) dimers on a xanthene scaffold, J. Phys. Chem. A 117 (40) (2013) 10333–10345.

[16] D. Parida, P.D. Pancharatna, M.M. Balakrishnarajan, On the origin of photodynamic activity of perylene quinone framework, Xxvii Iupap Conference on Computational Physics (Ccp2015) 759 (2016).

[17] M.A. Filatov, S. Karuthedath, P.M. Polestshuk, S. Callaghan, K.J. Flanagan, T. Wiesner, F. Laquai, M.O. Senge, BODIPY-pyrene and perylene dyads as heavy-atom-free singlet oxygen sensitizers, ChemPhotoChem (2) (2018) 1–11.

[18] E.R. dos Santos, J. Pina, T. Venancio, C. Serpa, J.M.G. Martinho, R.M. Carlos, Photoinduced energy and electron-transfer reactions by polypyridine ruthenium(II) complexes containing a derivatized perylene diimide, J. Phys. Chem. C 120 (40) (2016) 22831–22843.

[19] P. Spenst, R.M. Young, M.R. Wasielewski, F. Wurthner, Guest and solvent modulated photo-driven charge separation and triplet generation in a perylene bisimide cyclophane, Chem. Sci. 7 (8) (2016) 5428–5434.

[20] L. Flamigni, A. Zanelli, H. Langhals, B. Bock, Photophysical and redox properties of perylene bis- and tris-dicarboximide fluorophores with triplet state formation: transient absorption and singlet oxygen sensitization, J. Phys. Chem. A 116 (6) (2012) 1503–1509.

[21] H. Dincalp, S. Kizilok, S. Icli, Targeted singlet oxygen generation using different DNA-interacting perylene diimide type photosensitizers, J. Fluorescence 24 (3) (2014) 917–924.

[22] F. Yukruk, A.L. Dogan, H. Canpinar, D. Guc, E.U. Akkaya, Water-soluble green perylenediimide (PDI) dyes as potential sensitizers for photodynamic therapy, Org. Lett. 7 (14) (2005) 2885–2887.

[23] C. Kirmaier, E. Hindin, J.K. Schwartz, I.V. Sazanovich, J.R. Diers, K. Muthukumaran, M. Taniguchi, D.F. Bocian, J.S. Lindsey, D. Holten, Synthesis and excited-state photodynamics of perylene-bis(imide)-oxochlorin dyads. A charge-separation motif, J. Phys. Chem. B 107 (15) (2003) 3443–3454.

[24] P. Semeraro, G. Chimienti, E. Altamura, P. Fini, V. Rizzi, P. Cosma, Chlorophyll a in cyclodextrin supramolecular complexes as a natural photosensitizer for photodynamic therapy (PDT) applications, Mater. Sci. Eng. C-Mater. Biol. Appl. 85 (2018) 47–56.

[25] V. Rizzi, P. Fini, P. Semeraro, P. Cosma, Detailed investigation of ROS arisen from chlorophyll a/Chitosan based-biofilm, Colloids Surf. B-Biointerfaces 142 (2016) 239–247.

[26] X. Li, S. Lee, J. Yoon, Supramolecular photosensitizers rejuvenate photodynamic therapy, Chem. Soc. Rev. 47 (4) (2018) 1174–1188.

[27] V. Rizzi, D. Vurro, T. Placido, P. Fini, A. Petrella, P. Semeraro, P. Cosma, Gold-chlorophyll a-hybrid nanoparticles and chlorophyll a/cetyltrimethylammonium chloride self-assembled-suprastructures as novel carriers for chlorophyll a delivery in water medium: photoactivity and photostability, Colloids Surf. B-Biointerfaces 161 (2018) 555–562.

[28] I.O.L. Bacellar, T.M. Tsubone, C. Pavani, M.S. Baptista, Photodynamic efficiency: from molecular photochemistry to cell death, Int. J. Mol. Sci. 16 (9) (2015) 20523–20559.

[29] Y. Nosaka, A.Y. Nosaka, Generation and detection of reactive oxygen species in photocatalysis, Chem. Rev. 117 (17) (2017) 11302–11336.

[30] M. Bregnhoj, M. Westberg, B.F. Minaev, P.R. Ogilby, Singlet oxygen photophysics in liquid solvents: converging on a unified picture, Acc. Chem. Res. 50 (8) (2017) 1920–1927.

[31] C. Mari, H. Huang, R. Rubbiani, M. Schulze, F. Würthner, H. Chao, G. Gasser, Evaluation of perylene bisimide-based Ru^{II} and Ir^{III} complexes as photosensitizers for photodynamic therapy, Eur. J. Inorg. Chem. (2017) 1745–1752.

[32] M. Franceschin, A. Rizzo, V. Casagrande, E. Salvati, A. Alvino, A. Altieri, A. Ciammaichella, S. Iachettini, C. Leonetti, G. Ortaggi, M. Porru, A. Bianco, A. Biroccio, Aromatic core extension in the series of N-cyclic bay-substituted perylene G-quadruplex ligands: increased telomere damage, antitumor activity, and strong selectivity for neoplastic over healthy cells, ChemMedChem 7 (2012) 2144–2154.

[33] D. Bechet, P. Couleaud, C. Frochot, M.-L. Viriot, F. Guillemin, M. Barberi-Heyob, Nanoparticles as vehicles for delivery of photodynamic therapy agents, Trends Biothecnol. 26 (11) (2008) 612–621.

[34] A.A. Ghogare, J.M. Miller, B. Mondal, A.M. Lyons, K.A. Cengel, T.M. Busch, A. Greer, Fluorinated photodynamic therapy device tips and their resistance to fouling for in vivo sensitizer release, Photochem. Photobiol. 92 (1) (2016) 166–172.

[35] V. Sgobba, G. Giancane, D. Cannoletta, A. Operamolla, O.H. Omar, G.M. Farinola, D.M. Guldi, L. Valli, Langmuir-Schaefer films for aligned carbon nanotubes functionalized with a conjugate polymer and photoelectrochemical response enhancement, ACS Appl. Mater. Interfaces 6 (1) (2014) 153–158.

[36] S. Bettini, R. Pagano, L. Valli, G. Giancane, Spectroscopic investigation of the selective interaction of mercuric and cupric ions with a porphyrin active layer, J. Phys. Chem. C 118 (23) (2014) 12384–12390.

[37] G. Giancane, L. Valli, S. Sortino, Dual-function multilayers for the photodelivery of nitric oxide and singlet oxygen, ChemPhysChem 10 (2009) 3077–3082.

[38] L. Valli, G. Giancane, A. Mazzaglia, L.M. Scolaro, S. Conoci, S. Sortino, Photoresponsive multilayer films by assembling cationic amphiphilic cyclodextrins and anionic porphyrins at the air/water interface, J. Mater. Chem. 17 (17) (2007) 1660–1663.

[39] V. Kunz, V. Stepanenko, F. Wurthner, Embedding of a ruthenium(II) water oxidation catalyst into nanofibers via self-assembly, Chem. Commun. 51 (2) (2015) 290–293.

[40] S.J. Manning, W. Bogen, L.A. Kelly, Synthesis, characterization, and photophysical study of fluorescent N-substituted Benzo[ghi]perylene "Swallow Tail" Monoimides, J Org Chem 76(15) (2011) 6007–6013.

[41] R. Hertmanowski, E. Piosik, T. Martynski, Thermodynamic properties of Langmuir layers created of monoimide perylenetetracarboxylic acid derivatives, Phase Transitions 89 (4) (2016) 419–424.

[42] A. Terzi, E. Storelli, S. Bettini, T. Sibillano, D. Altamura, L. Salvatore, M. Madaghiele, A. Romano, D. Siliqi, M. Ladisa, L. De Caro, A. Quattrini, L. Valli, A. Sannino, C. Giannini, Effects of processing on structural, mechanical and biological properties of collagen-based substrates for regenerative medicine, Sci Rep-UK 8 (2018).

[43] Z.S.S. Bettini, R. Pagano, L. Dordević, L. Salvatore, M. Prato, G. Giancane, L. Valli, Perylene Bisimide aggregates as probes for subnanomolar discrimination of aromatic biogenic amines, ACS Appl. Mater. Interfaces 11(18) (2019) 17079–17089.

[44] F. Fischer, G. Graschew, H.J. Sinn, W. Maier-Borst, W.J. Lorenz, P.M. Schlag, A chemical dosimeter for the determination of the photodynamic activity of photosensitizers, Clin. Chim. Acta 274 (1) (1998) 89–104.

[45] B.M. Cellamare, P. Fini, A. Agostiano, S. Sortino, P. Cosma, Identification of ROS produced by photodynamic activity of chlorophyll/cyclodextrin inclusion complexes, Photochem. Photobiol. 89 (2) (2013) 432–441.

[46] V. Rizzi, P. Fini, F. Fanelli, T. Placido, P. Semeraro, T. Sibillano, A. Fraix, S. Sortino, A. Agostiano, C. Giannini, P. Cosma, Molecular interactions,

characterization and photoactivity of Chlorophyll *a*/chitosan/2-HP-β-cyclodextrin composite films as functional and active surfaces for ROS production, Food Hydrocolloids 58 (2016) 98–112.
[47] T. Mosmann, Rapid colorimetric assay for cellular growth and survival: application to proliferation and cytotoxicity assays, J. Immunol. Methods 65 (1–2) (1983) 55–63.
[48] S. Bettini, D. Vergara, S. Bonsegna, L. Giotta, C. Toto, M. Chieppa, M. Maffia, G. Giovinazzo, L. Valli, A. Santino, Efficient stabilization of natural curcuminoids mediated by oil body encapsulation, RSC Adv. 3 (16) (2013) 5422–5429.
[49] W. Wang, J.J. Han, L.Q. Wang, L.S. Li, W.J. Shaw, A.D.Q. Li, Dynamic pi-pi stacked molecular assemblies emit from green to red colors, Nano Lett. 3 (4) (2003) 455–458.
[50] W.E. Ford, Photochemistry of 3,4,9,10-perylenetetracarboxylic dianhydride dyes – visible absorption and fluorescence of the di(glycyl)imide derivative monomer and dimer in basic aqueous-solutions, J. Photochem. 37 (1) (1987) 189–204.
[51] P.A. Korevaar, C. Schaefer, T.F.A. de Greef, E.W. Meijer, Controlling chemical self-assembly by solvent-dependent dynamics, J. Am. Chem. Soc. 134 (32) (2012) 13482–13491.
[52] R.F. Fink, J. Seibt, V. Engel, M. Renz, M. Kaupp, S. Lochbrunner, H.-M. Zhao, J. Pfister, F. Würthner, B. Engels, Exciton trapping in π-conjugated materials: a quantum-chemistry-based protocol applied to Perylene Bisimide dye aggregates, J. Am. Chem. Soc. 130 (2008) 12858–12859.
[53] C.D. Shang, L. Wang, Y.Q. An, P. Chen, X.M. Chang, Y.Y. Qi, R. Kang, Y. Fang, Langmuir-Blodgett films of perylene bisimide derivatives and fluorescent recognition of diamines, PCCP 19 (35) (2017) 23898–23904.
[54] S. Yagai, T. Seki, T. Karatsu, A. Kitamura, F. Wurthner, Transformation from H- to J-aggregated perylene bisimide dyes by complexation with cyanurates, Angew. Chem. Int. Ed. 47 (18) (2008) 3367–3371.
[55] E.E. Neuteboom, S.C.J. Meskers, E.W. Meijer, J.R.A. J., Photoluminescence of self-organized perylene bisimide polymers, Macromol. Chem. Phys. 205 (2004) 217–222.
[56] X. Xu, A. Austin, S.E. Mylon, J. Plenge, J.M. Szarko, Improving the quantum yields of Perylene Diimide aggregates by increasing molecular hydrophobicity in polar media, ChemPhysChem 18 (18) (2017) 2430–2441.
[57] D. Bauman, R. Hertmanowski, K. Stefańska, R. Stolarski, The synthesis of novel perylene-like dyes and their aggregation properties in Langmuir and Langmuir-Blodgett films, Dyes Pigm. 91 (2011) 474–480.
[58] R. Hertmanowski, T. Martynski, D. Bauman, Alignment of molecules in Langmuir and Langmuir-Blodgett films of binary mixtures of 3,4,9,10-tetra-(n-alkoxy-carbonyl)-perylenes with a liquid crystal, J. Mol. Struct. 741 (1–3) (2005) 201–211.
[59] L. Valli, S. Casilli, L. Giotta, B. Pignataro, S. Conoci, V.V. Borovkov, Y. Inoue, S. Sortino, Ethane-bridged zinc porphyrin dimers in Langmuir-Shafer thin films: structural and spectroscopic properties, J. Phys. Chem. B 110 (10) (2006) 4691–4698.
[60] F. Naso, F. Babudri, D. Colangiuli, G.M. Farinola, F. Quaranta, R. Rella, R. Tafuro, L. Valli, Thin film construction and characterization and gas-sensing performances of a tailored phenylene-thienylene copolymer, J. Am. Chem. Soc. 125 (30) (2003) 9055–9061.
[61] M.S. Choi, One-dimensional porphyrin H-aggregates induced by solvent polarity, Tetrahedron Lett 49 (49) (2008) 7050–7053.
[62] K. Saito, H-aggregate formation in squarylium Langmuir-Blodgett films, J. Phys. Chem. B 105 (19) (2001) 4235–4238.
[63] G. Giancane, A. Ruland, V. Sgobba, D. Manno, A. Serra, G.M. Farinola, O.H. Omar, D.M. Guldi, L. Valli, Aligning single-walled carbon nanotubes by means of Langmuir-Blodgett film deposition: optical morphological, and photo-electrochemical studies, Adv. Funct. Mater. 20 (15) (2010) 2481–2488.
[64] G. Sauerbrey, Verwendung von Schwingquarzen zur Wägung dünner Schichten und zur Mikrowägung, Zeitschrift für Physik 155 (2) (1959) 206–222.
[65] G. Bussetti, A. Violante, R. Yivlialin, S. Cirilli, B. Bonanni, P. Chiaradia, C. Goletti, L. Tortora, R. Paolesse, E. Martinelli, A. D'Amico, C. Di Natale, G. Giancane, L. Valli, Site-sensitive gas sensing and analyte discrimination in Langmuir-Blodgett porphyrin films, J. Phys. Chem. C 115 (16) (2011) 8189–8194.
[66] L. Gazzera, C. Corti, L. Pirrie, A. Paananen, A. Monfredini, G. Cavallo, S. Bettini, G. Giancane, L. Valli, M.B. Linder, G. Resnati, R. Milani, P. Metrangolo, Hydrophobin as a nanolayer primer that enables the fluorinated coating of poorly reactive polymer surfaces, Adv. Mater. Interfaces 2 (14) (2015).
[67] R. Mendelsohn, C.R. Flach, Infrared reflection-absorption spectroscopy of lipids, peptides, and proteins in aqueous monolayers, Peptide-Lipid Interactions 52 (2002) 57–88.
[68] R.B. Silverstein, G.C. Bassler, M. T.C., Spectrometric Identification of Organic Compounds, 4th ed., 1981.
[69] Y.W. Yi Cui, Yu Liu, Gaomai Yang, Lixin Liu, Hongbing Fu, Zhibo Li, Shu Wang, Zhaohui Wang, Yongming Chen, PEGylated nanoparticles of diperylene bisimides with high efficiency of $^1O_2$ generation, Dyes Pigm. 97 (2013) 129–133.